공학석사 학위논문

Electrocardiographic signal processing for respiration signal detection & heart rate variability analysis

호흡수 측정과 심박변이 분석을 위한 심전도 신호 처리

2014년 8월

The Graduate School Seoul National University

Dept. of Electrical and Computer Engineering

Joaquin Sanchez Duarte

호흡수 측정과 심박변이 분석을 위한 심전도 신호 처리

Electrocardiographic signal processing for respiration signal detection & heart rate variability analysis

지도 교수 서 종 모

이 논문을 공학석사 학위논문으로 제출함
2014 년 8 월

서울대학교 대학원
전기컴퓨터공학부
Joaquin Sanchez Duarte

Joaquin Sanchez Duarte의 공학석사 학위논문을
인준함
2014 년 8 월

위 원 장 _____ 김 성 준 _____ (인)

부위원장 _____ 서 종 모 _____ (인)

위   원 _____ 권 성 훈 _____ (인)

Abstract

The aim of this thesis is to present electrocardiographic signal processing methods for the extraction of relevant cardiovascular and respiratory information. Different signal processing techniques are presented; non real-time wavelet transform and real-time signal processing methods, both with the aim of the extraction of the QRS complex. Further, the respiration signal is derived using a plethysmography techniques solely based on the impedance changes of the thorax during respiration and finally the relationships between the cardiorespiratory and the autonomic nervous system is explored. Closely examining the heart rate, respiration and changes of the heart beat during respiration can provide enough information to evaluate the autonomic nervous system and so a health status of the patient.

Key Words : electrocardiographic signal, respiration signal, real-time, wavelet transform, pan & tompkins

Sudent Number : 2012-23961

Contents

Glossary

ANS Autonomic Nervous System. 27

AV Node Atrioventricular node. 1–3

CWT Countinous Wavelet Transform. 12

Diastole The phase of the heartbeat when the heart muscle relaxes and allows the chambers to fill with blood. 3

DWT Discrete Wavelet Transform. 12

ECG Electrocardiogram. 1, 3

EDR Electrocardiographic Derived Respiration. 19

FT Fourier Transform. 11

HRV Heart Rate Variability. 27, 28

MEA Mean Electrical Axis. 20, 25

PC Parasympathetic Control. 34

PNS Parasympathetic Nervous System. 27, 28

RSA Respiration Sinus Arrhythmia. 27

SA Node Sino atrial node. 1, 3, 30

SNS Sympathetic Nervous System. 27, 28

STFT Short Term Fourier Transform. 11

Systole the phase of the heartbeat when the heart muscle contracts and pumps blood from the chambers into the arteries. 3

WT Wavelet Transform. 12, 21

List of Tables

List of Figures

Chapter 1

The Electrocardiogram

1.1 ECG/EKG

The electrocardiogram is a voltage measurement on the chest that is generated by the electric depolarization and repolarization of the heart. The ECG represents an extracellular electric behavior of the cardiac muscle tissue, measured as the sum of all the actions potentials from the heart detected on the surface of the body. The ECG is an indirect indicator of heart muscle contraction as the action potentials are a direct cause of the contractions

1.1.1 Activation of the Heart

The rhythmic contractions of the heart depend on electrical pulses generated at the Sino atrial node (SA Node), located at the right atrium of the heart, and commonly known as the heart's natural pacemaker. The propagation of the action impulse starts at the SA Node and propagates through the atria and arriving to the Atrioventricular node (AV Node), the boundary between the atria and the ventricles, the AV Node provides an electrical path between the two. The self-excitatory cells in the SA Node generate an action potential at a rate of approximately 70 per minute, the highest rate of the self-excitatory cells in the heart, and therefore it sets the activation frequency of the whole

heart [11]. Ventricular excitation follows atrial excitation after a delay in the AV Node. This delay permits completion of atrial contraction ventricular filling, before ventricular contraction. The cardiac muscle cells activate by the depolarization of the membrane due to the inflow of sodium ions; the potential inside the cell becomes more positive with respect to the potential outside the cell; and then return to their the resting state (-90mV with respect to the outside of the cell) by the outflow of potassium ions. The voltage change or pulse is known as 'Action potential'. This action potential of cardiac cells is generated exactly the same way as in nerve cells with the main difference being that the duration of the cardiac muscle impulse is twice longer. Depolarization is a propagating phenomenon; the electric field produced when a cell depolarizes will trigger the depolarization of the next cell and so on. On the contrary repolarization is not a propagation phenomenon and occurs naturally after depolarization. In ventricular muscle the outer surface epicardial cells, have shorter action pulse than the inner surface endocardial cells. Therefore, repolarization would seem to be travelling from epicardium to endocardium, in the opposite direction to that of activation[11]. Once depolarization waves reach the ventricles, a wavefront propagates through the ventricular mass toward the outer wall causing mechanical contraction. The processes explained above represent the activity of the heart at an intracellular level [16].

1.1.2   Cardiac Conduction Cycle

The hearts own electrical system helps the heart contract and relax in a coordinated, rhythmic fashion. This property of the heartbeat is called synchrony. Automacity of the pacemaker cells is the ability to depolarize in the absence of external stimulation [11], these cells are distributed through the heart and are responsible for the excitation of the Myocardiocytes cells which make up the atria and ventricles. These cells must be able to shorten and lengthen their fibres, and the fibres must be flexible enough to stretch.

The cardiac cycle start with the depolarization of the atria due to action potentials spreading from the SA Node node to the AV Node causing atrial muscle cells to depolarize and contract. This phase is known as the Atrial systole, on the ECG this is represented by the P-wave. The QRS complex is produced by ventricular depolarization and is the result of Septal depolarization, Apical depolarization and Late left ventricular depolarization; also called Ventricular systole. Repolarization of the Atria, or Atrial Diastole, occurs during ventricular Systole but activity of the atria is momentarily hidden by the QRS complex in the ECG. Finally repolarization of the ventricle happens when the ventricular walls relax and recover after contraction, a period also called ventricular diastole; this is shown by the T-wave in the ECG.

The 0V region traces on the ECG, Figure 1.1, are; the PR interval being caused mainly by conduction delay in AV Node and the ST segment, that is related to the average duration of the plateau regions of individual ventricular cells when the ventricles are depolarized. The total time for the depolarization and repolarization of the ventricles to occur is commonly referred as QT interval. Figure 1.1 shows a typical labeled ECG trace; the result of the coordinated electrical system of the heart measured in the thoracic area of a healthy individual.

1.2 System of Leads

Potential differences between two electrodes placed in the surface of the body are caused by the electrical signals of the heart. When performing an ECG by measuring these voltages; the heart is modeled as a net equivalent dipole whereby the magnitude and orientation of this dipole changes during the course of the conduction cycle. We will assume that the thorax is a volume conductor, a purely passive conductor containing no electric sources or sinks [23]. The net equivalent dipole of the heart is further represented by its dipole moment, named the Cardiac vector (a vector directed from positive to nega-
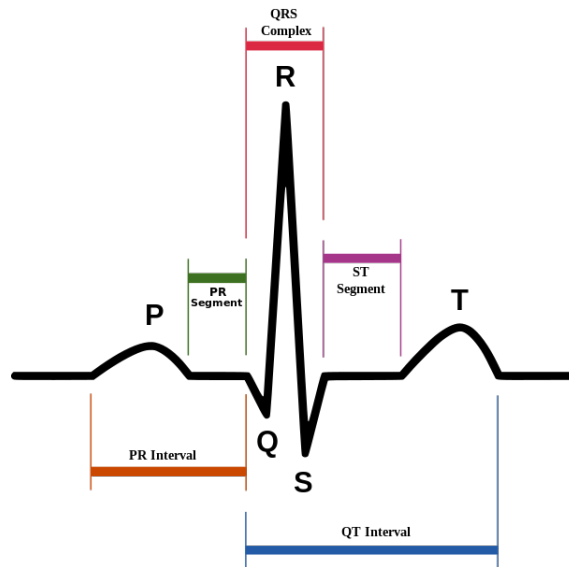
Figure 1.1: ECG waveform with its features

tive and having a magnitude proportional to the amount of charge multiplied by the separation of the two charges). Returning to the measured voltage on the surface of the thorax, a 'lead vector' is given between a pair of electrodes; the direction of this unit vector is defined by the cardiac vector's direction that produces the highest voltage at that particular lead. In vector algebra the potential is equal to the dot product between the cardiac vector M and the lead vector c.

$$\Phi_P = M \cdot c \qquad (1.1)$$

This type of lead is referred to as a bipolar lead, because neither electrode is remote. In other words when a wave of depolarization travels parallel to the lead vector a maximal voltage will appear at the lead. If on the other hand, the two leads are perpendicular to each other and the cardiac vector is parallel to one lead, only one lead will show maximal deflection while the other stays at 0V. Therefore the deflections of the ECG will be different for every lead because each of the leads will "see" the sequence of depolarization vectors from a different perspective; the direction of the cardiac vector relative

to the recording electrode placement determines, in part, the magnitude of the recording voltage. Leads placed strategically on the body, permits the direction of the cardiac vector during the conduction cycle to be calculated.

1.2.1 Einthoven's triangle

More than one lead is used in clinical ECG to be able to describe the activity of the heart fully. Three basic leads make up the frontal-plane ECG. Usually the electrodes are placed in the right arm (RA), left arm (LA), and the left leg (LL): forming Lead I (from LA to RA) Lead II (LL to RA) and Lead III (from LL to LA), this combination of leads can be described, as shown in Figure 1.2, by forming an equilateral triangle known as Einthoven's triangle. Equation 1.2 are the three voltages that are measured by the leads, expressed in vector form with their corresponding leads vectors.
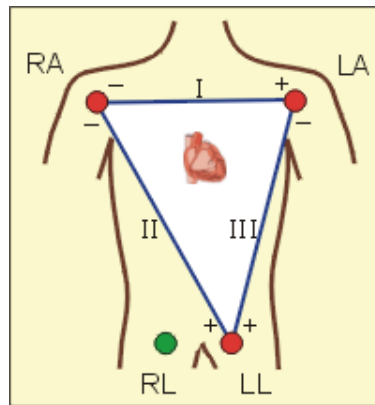
Figure 1.2: Basic electrocardiogram leads placement

$$V_I = c_I \cdot pV_{II} = c_I I \cdot pV_{III} = c_I II \cdot p \qquad (1.2)$$

1.3 Instrumentation

The acquisition of the ECG signal is rather difficult; the signal that appears at the electrodes is a few millivolts and has a very low bandwidth of no more

than 150Hz. Bed-side monitoring ECG monitors use a 3-lead system to acquire the ECG signal. Three lead systems are usually used as transport monitors and usually monitor two areas of the heart; the lateral and the inferior. Limb lead II is the most common monitoring lead configuration, because it normally produces the largest amplitude QRS segment.

1.3.1   Sources of noise

Interference

The main source of interference is the AC mains power supply, The ECG signal is superimposed with a much larger external high frequency noise plus 50/60Hz interference normal mode; the number power lines can be prominent in the recording environment and so introduce a fair amount of noise when coupling with ECG circuitry, the electrodes and the patient itself. This coupling is caused by stray capacitances, which can be large for instance, 1pF at 50Hz. Shielding the leads and grounding the shields can mitigate this type of interference.

Common Mode Voltage

The current that flows through the body from the power line, displacement current, produces a common-mode voltage v_{cm} that appears throughout the body. The common mode input to the amplifier is given by 1.3 . An ideal differential amplifier would completely reject this voltage but in reality, the output has some dependence on the average of v_+ and v_- .

$$v_c = \frac{v_+ + v_-}{2} \tag{1.3}$$

In real, non-ideal amplifiers

$$v_{out} = A_d v_v \pm A_c v_c \tag{1.4}$$

Where Z_1 and Z_2 are the impedances of the first and second electrode respectively. Based in this equation a large Z_{cm} compared to Z_1 and Z_2 would reduce the common mode voltage component at the output. Making the electrode impedances equal would eliminate the second term of the equation; however, the impedance would depend on the position of the electrode and also more intrinsic artifacts such as the motion of the patient. Regardless, electrode impedances should be kept as low as possible [1].

Instrumentation Amplifier

The three op-amp instrumentation amplifier is comprised, U1, U2 and U3, as shown in Figure 1.3. U1 and U2 act as non-inverting amplifiers providing high input impedance. U3 is a unity gain amplifier and rids of the common mode at its output. The proceeding stage provides the required filtering in the form of a passive high-pass filter; C1 and R8; and an active low-pass at the output of the amplifier. Currently there is a wide availability of in-chip instrumental amplifiers; some of these are designed with bio-signals in mind for medical instrumentation; therefore, deliver excellent characteristics such as high CMRR. The circuit in Figure 1.3 serves the purpose to illustrate one of possible implementations of the analog front end of an ECG system.

1.3.2   Bio-acquisition hardware

We opted for a high performance data acquisition device; the Texas instruments ADS1299 evaluation board was interfaced with an Arduino Due. Figure 1.4 is a block diagram of this arrangement. A PCB was designed to fit in both boards, as shown in Figure 1.5. The ADS1299, originally designed for Electroencephalography measurements has 8 inputs, each of which has a programable gain amplifier, PGA, with a very low input referred noise of $1.0\mu V_{pp}$. High fidelity signals were obtained due to the high resolution, 24bits per channel, and the use of a right leg drive electrode which helped mitigate noise. The

sampling rate was 500Hz and data was collected with the Arduino via serial

parallel interface protocol, SPI, and transferred to a PC via USB-parallel port.

All the data processing was done using MATLAB as well as all the plots shown

in this document.

11
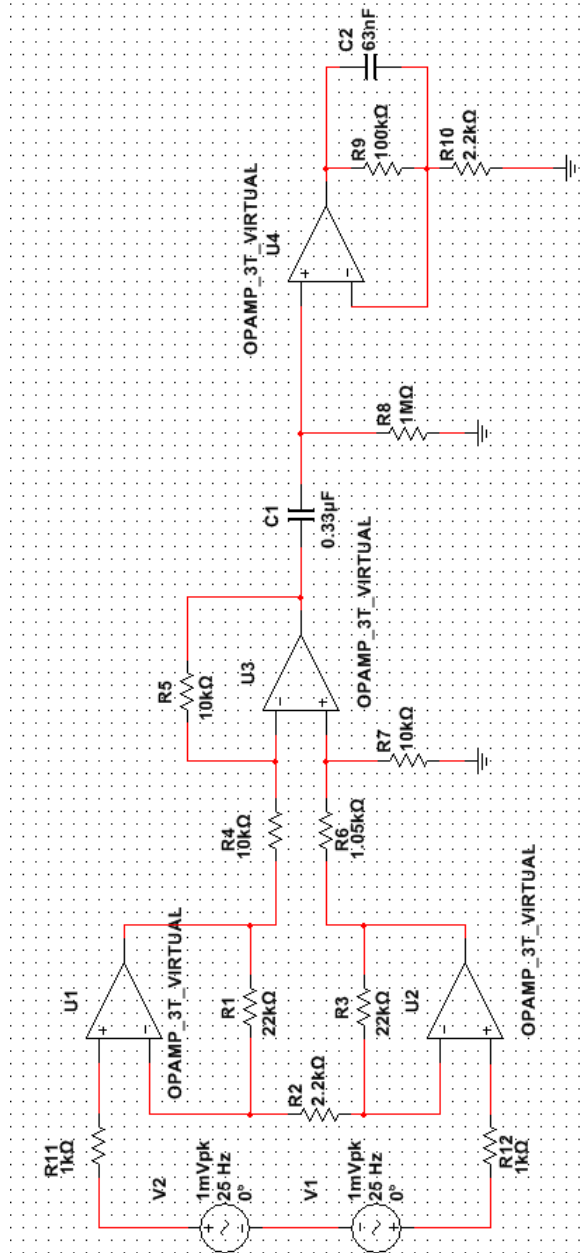
Figure 1.3: 3-Opamp instrumentation amplifier.
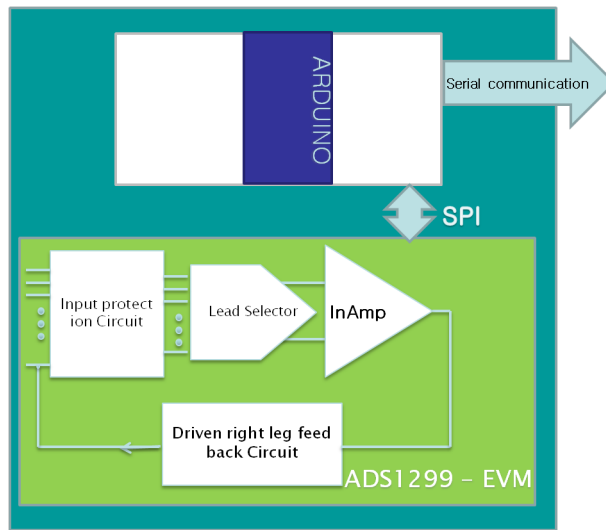
Figure 1.4: Data acquistion device block diagram
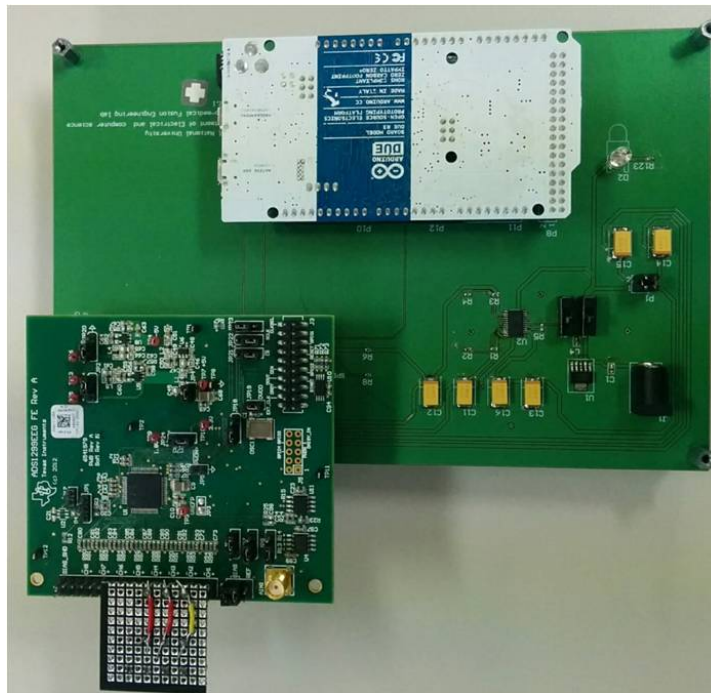
Figure 1.5: PCB board with ADS and Arduino

Chapter 2

ECG processing with Wavelet Transforms

In Fourier Transform (FT), in dealing with stationary signals - signals which do not change their frequency in time - the transform will give us perfect frequency resolution, that is, it will tell us what frequencies exist in the signal; if the signal suddenly changes its frequency during its existence in time, that is, it ceases to be stationary, the FT is incapable of providing any time resolution and tell us the time the signal changes its frequency content. The reason for this, is that the kernel function of the FT, the exponential function $e^{j\omega t}$, lasts from minus to plus infinity. The Short Term Fourier Transform (STFT), using a finite window length, are able to provide better frequency resolution at the cost of poorer time resolution. Since almost all biological signals are stationary, i.e, ECG, EEG EMG, the FT serves no purpose in determining which frequency components occur at which times. Low frequencies are better resolved in frequency and high frequencies in time since a higher number of samples in any interval are better resolved in time, therefore using a single window length in STFT will provide either good or bad frequency resolution for either high or low frequencies depending on the size of the window. This limitation of STFT is the main reason we now discuss Wavelet Transforms

2.1 Continous Wavelet transform CWT

In equation 2.1, a function *f(t)* is transformed by a function Ψ that is shifted by τ, the translation parameter and scaled by *a*. This function is refered to as the mother wavelet. Wavelets are "small waves" which are oscillatory with fast decaying to zero in nature.

$$[W_\Psi f(t)](\tau, a) = \int_{-\infty}^{\infty} f(x) \frac{1}{\sqrt{a}} \Psi^*((t-\tau)/a) \, \mathrm{d}t = W_\Psi f(a, \tau) \quad ; a \neq 0 \quad (2.1)$$

In Countinous Wavelet Transform (CWT), a set of scaled and translated functions, $\Psi_{\tau,a}$, derived from the mother wavelet, Ψ, provide the resolutions needed to resolve the signal at different frequencies. A wavelet at a low scale is good for resolving high frequencies whereas the global information of the signal (low frequencies) are better resolved at higher scales. The result of the transform are a set of wavelet coefficients $W_\Psi f(\tau, a)$ which represent how well the signal *f*, correlates with the particular wavelet at τ and *a*. To summarise, Wavelet Transform (WT) has a good time and poor frequency resolution at high frequencies, and good frequency and poor time resolution at low frequencies.

2.2 Discrete Wavelet Transform DWT

Discrete Wavelet Transform (DWT) is a fast algorithm for machine computation [17]. Since the CWT is not often employed [20], DWT is more frequently applied than its continuous counterpart. The variables τ and *a* are discretized. Dyadic sampling of the scaling parameter is normally chosen therefore $a = 2^j$. The resultant resolution of the DWT is a grid like structure with frequency on the y-axis and time on the x-axis [2]. Rectangles on the low scales (high frequencies) part of the grid have short time duration for higher time resolution

but lower frequency resolution; good for high frequencies and the rectangles near the origin have longer time durations for better low frequency resolution.

2.2.1 Multi Resolution Analysis with Discrete Wavelet transforms

Multiresolution analysis allows the analysis of the signal at different frequencies with different resolutions.The subband coding algorithm, Figure 2.1, permits the decomposition of the signal into a set of discrete frequency ranges. This algorithm relies on the DWT which utilises multiresolution filter banks and special wavelet filters for the analysis and reconstruction of signals [12]. For a simple explanation of how the algorithms performs, imagine we have a signal whose maximum frequency is π, We will pass the signal through a series of low pass, $H(z)$ and high pass filters $G(z)$ which result in two signals, one whose frequency range is $0 - \pi/2$ and the other is $\pi/2 - \pi$. After this operation the amount of data is doubled and hence the output of each filter is downsampled, $\downarrow 2$ by a factor of two, that is, we remove half the samples to produce the desired time dilation. The outputs of the first set of filter banks are referred to as the first detail coefficient cD_1 and the first approximation coefficient, cA_1, at the high pass filter and low pass filter outputs respectively.

The filtering operation is repeated on the approximation coefficient, see Figure 2.1. We perform this decomposition until we reach the required resolution. By decomposing the signal in this manner we are able to see different parts of the signal by adjusting the level of decomposition. One key point worth mentioning is the importance of the choice of wavelet, this choice has to have into account the morphology of the ECG signal and have similar characteristics [24].
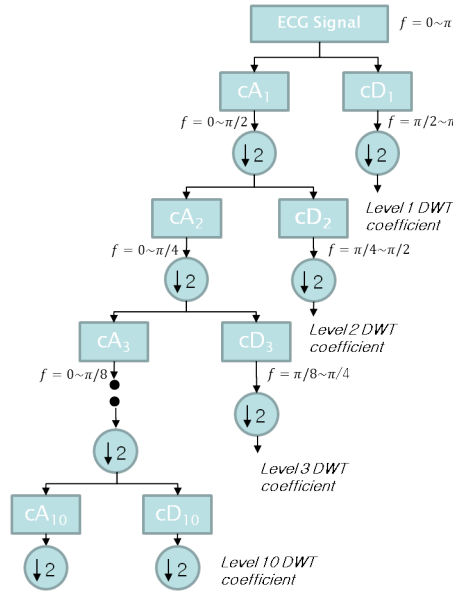
Figure 2.1: Sub-Band Coding

2.2.2 ECG Decomposition

One important property from algorithm described above, is that the signal can be reconstructed back from the wavelet coefficients [12]. Figure 2.2 shows an example of an arbitrary ECG being decomposed into five wavelet coefficients and then each of those coefficients being singularly reconstructed and plotted. It is possible to reconstruct the signal without some of the coefficients by either thresholding the coefficients or removing them all together. In the next section we will see how this is relevant for ECG signal processing.

2.2.3 Denoising with Wavelet Transforms

Denosing is only a matter of performing an inverse transform without the DWT components that are considered to contain the noise in the signal. As shown in Figure 2.2 the highest wavelet coefficient aD_{12} contains the lowest frequencies range, 0.06 - 0.12Hz, and the first one, cD_1, contains frequencies from 125-250Hz. Normally ECG relevant information is contained within the 0.5-100Hz frequency range. This constraint dictates that the aforementioned coefficients contain noise; either low frequency baseline wandering noise, or
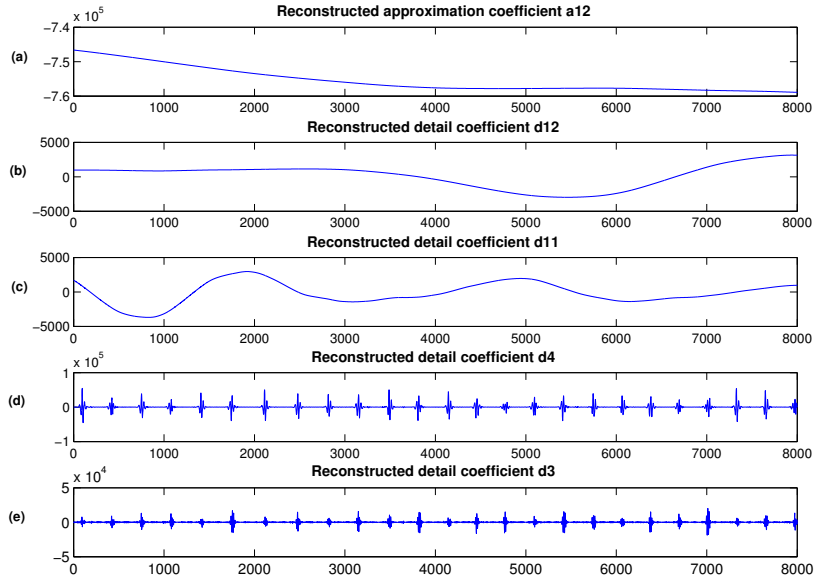
Figure 2.2: Decomposition

higher frequency artifacts that permeate the recordings. Many authors have
[7],[20],[24], [2] have taken advantage of this frequency selectivity to perform
denosing and, as we will see later, feature extraction. In Figure 2.3 the first
plot corresponds to the raw ECG signal without any processing done, next we
remove coefficients cD_1 to remove the high frequency noise and subsequently
the last plot has been done by reconstructing back the signal without cD_{12}.
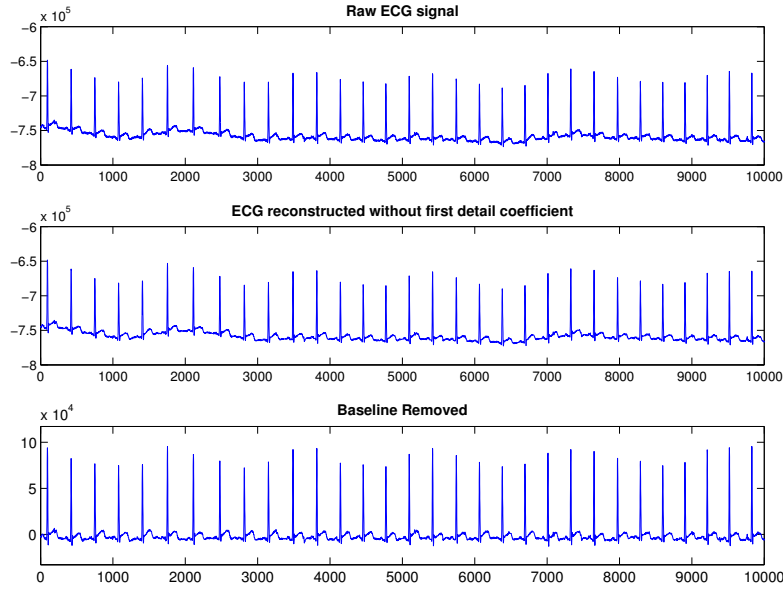
Figure 2.3: Denoising

Another common technique, although I found it unnecessary dude to the high quality of the data, is to further threshold the wavelet coefficients before signal reconstruction. Hence, once the coefficients are found one can set a threshold at each of the transform's levels. If the coefficients that are smaller than the value of the threshold those coefficients are simply discarded. Reference to this method can be found in the following papers; [2] and [12].

2.2.4 QRS complex Detection

The graph shown in Figure 2.4 is a plot of the QRS power spectra, taken from the work by N.V Thakor et al.[21]. From this we can derive that the QRS power spectra covers approximately a range from 5 to 40Hz, above the frequency range that the P-T waves covers.
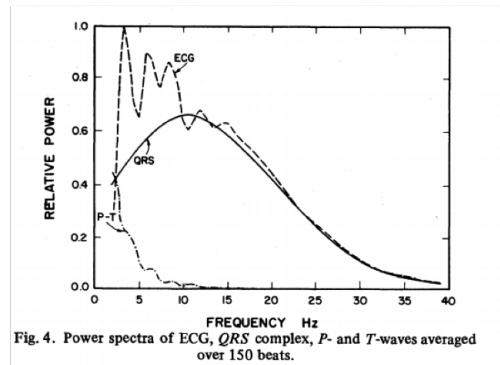
Figure 2.4: QRS Compex Spectra

With this information a simple QRS detector based on the suband algorithm was developed. At a sampling rate of 500Hz, wavelet coefficients cD_3, Figure 2.5 containing information from the signal at frequencies from 32.25-62.5Hz; in combination with a simple peak detector, successfully located the R-peaks of the QRS complex. The wavelet algorithm developed worked offline; once the data was stored and denoised using the methods described in the previous sections.
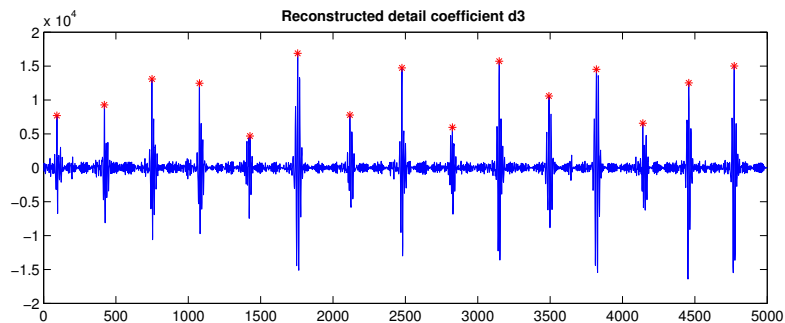
Figure 2.5: Reconstructed cD3 level coefficients

In most cases where the 3-lead ECG was recorded, with data up to 5 minutes long, the algorithm performed satisfactorily with a very few false detections and missed peaks. The short segment of an ECG after this operation was performed is shown in Figure 2.6, all the R-peaks of this segment were detected and emphasised with red circles.
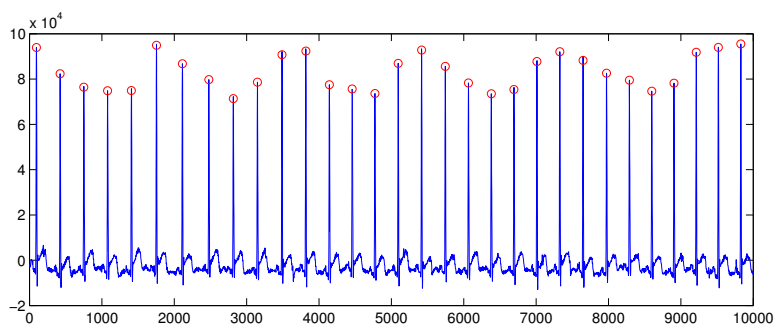
Figure 2.6: R peaks circled in red

Chapter 3

ECG Derived Respiration EDR

Respiration is vital for cellular life and therefore essential for animals. In humans respiration wouldn't be possible without the inhalation and exhalation of air in the lungs; breathing is accompanied by the movement muscles in the thorax which allow pressure changes inside the lungs and hence the flow of air in and out of them. The heart itself plays an important part as it pumps deoxigenated blood into the lungs as well as collect oxygenated blood from the lungs to circulate through the body.

Indirect and unobtrusive measurements of the respiratory signal can be extremely useful in the diagnosis of sleep disorders. For instance Sleep apnea, affect a large fraction of the population and can lead to a wide range of health problems such as decreased alertness, cardiovascular disease, high blood pressure and diabetes. Moddie has demonstrated that Electrocardiographic Derived Respiration (EDR) can help diagnose central and mixed apneas, and tachypnea with a certain degree of accuracy.

3.1 Impedance Plethysmography

It has to become clear to the reader that ECG derived respiration does not measure any of the functional lung volumes but provides information about the breathing motion by using the Electrocardiography signals

The measurement of the respiration signal via ECG, or EDR, is based on the changes of the transthoracic impedance at electrodes and this in turn influences the ECG signal recorded. Notice in Figure 3.1 the evident variation of the magnitude of the R-peaks due to impedance changes caused by respiration. If two orthogonal leads, corresponding to two orthogonal planes, placed in the chest, such as the ones that captured the signals below, were used to generate the Mean Electrical Axis (MEA) then it would appear as if modulated by motion of breathing and according to Moody, axial variations correspond well to recorded measurements of chest impedance. [15]
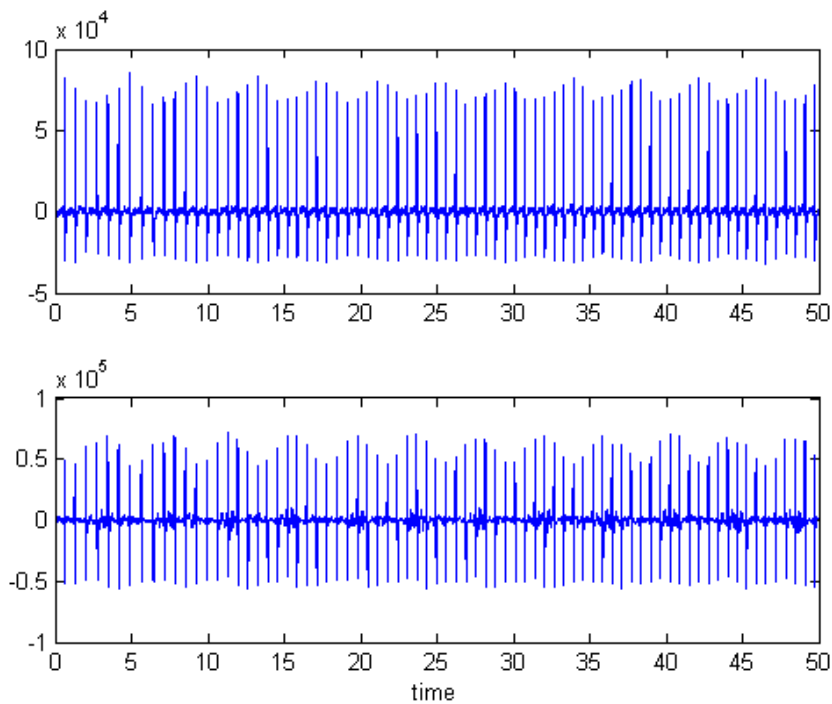
Figure 3.1: Lead II and MCL1 lead recorded for 50 seconds

3.2 Mean Cardiac axis

To process the MEA orientation to derive the respiration signal, the QRS complexes of the ECG have to be detected, in other words the QRS serves as a respiration signal sampling function. Since the respiration rate varies between 12 - 22 breaths per minute, we can safely assume that at the heart rate, which varies between 60- 100 bpm, can sample the respiration without loss of information. Heart rate is normally measured between QRS complexes so the challenge presented was to detect the complex in a real time fashion to derive a live EDR signal. Equation below shows the calculation needed to derive the MEA at any one QRS complex.

The MEA orientation between the Frontal and transverse plane can be derived with Lead II and modified chest lead I, MCL1. The MCL1 lead corresponds to an electrode at the 4th intercoastal space to the right of the sternum and a LA placed in the chest close to the shoulder. The MCL1 lead gives the best results when measuring at the supine position.

$$MEA(\theta) = tan^{-1} \frac{Area\ of\ QRS\ in\ Frontal\ Plane}{Area\ of\ QRS\ in\ Transverse\ plane} \quad (3.1)$$

3.3 Real time QRS Complex detection

As previously demonstrated in Section 2.2.4, using WT we successfully detected the R-peaks in an offline fashion. In this section we describe a different approach that suits the live detection of the MEA which, will be done at the QRS complex of the ECG signal. Therefore a real time, reliable and accurate QRS detection algorithm is required to perform this task. Numerous algorithms for QRS detection have been described over the past 30 years. Over time, more emphasis was placed in the algorithm's accuracy rather than in their complexity and computational load. For our application we needed an algorithm which could be implemented on a live data load. Hence we based

out algorithm on the preprocessing done by Pan and Tompkins.[18].

3.3.1 Pre-Processing

The Pan and Thompkins pre-processing algorithm is done in several different stages.

Band Pass Filter:

The aim of this first stage is try to filter out ECG components outside the QRS spectral range. Pan and Thompkins devised a bandpass filter made up two filters; a low pass with a cut-off of 12Hz and a high pass filter with a cut-off of 5Hz. These particular filters were realised with integer coefficient in their constant coefficient difference equations which results in better performance for live data processing. Without restrictions in terms of processing power, and with a different QRS spectral range definition, now from 5 - 25Hz , we opted for a Butterworth bandpass filter. This filter performed satisfactorily with an attenuation of 20dB at 2Hz on the highpass side and 20bB at the low-pass side.

Differentiator: Performs the derivative operation linearly in the frequency range of interest

$$H(z) = 1/8(-z^{-2} - 2z^{-1} + 2z^{1} + z^{2})$$
(3.2)

Squaring: Point by point squaring,

$$y(n) = x(n)^2$$
(3.3)

Point To Point Integration:

This is a moving window averager, it takes the first samples and adds a buffer of 74 zeros at the beginning of it.

$$y(n) = \frac{1}{74} \sum_{i=0}^{74} x(n-i) \qquad (3.4)$$

3.3.2   Peak Detection:

For each QRS complex, a distinguishable and elongated peak relative to the QRS is produced, as shown below in Figure 3.2. Its symmetry allows for easy detection and placement of fiducial marks on: the start of the peak, the middle of the peak and the crest of the peak. Correspondingly, on the ECG these points are: the start of the QRS complex, marked in green; the S-point of the QRS complex, marked in red; and the point just before the T-wave of the ECG, marked in pink.
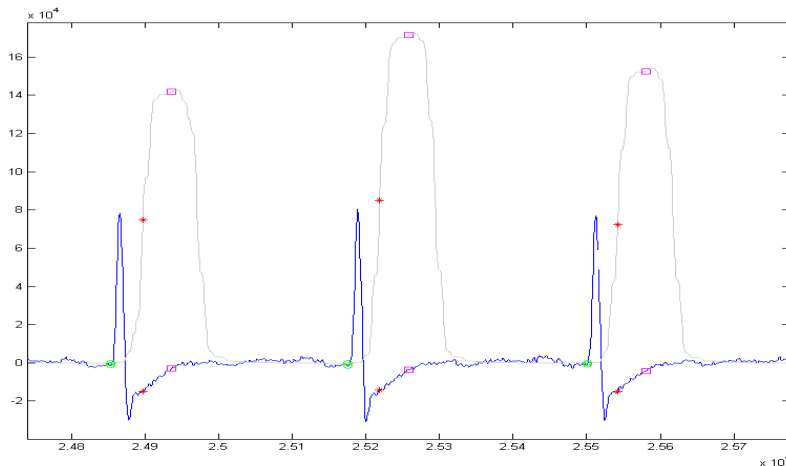
Figure 3.2: ECG, blue and Processed Signal, grey

Aside from finding the peaks in the processed signal, a peak sorting algorithm, for which a block diagram is shown in Figure 3.3, was used to improve the R-peak detection rate. At the start, a two second learning period is used to calculate a signal and a noise threshold which will be used to determine if the detected peaks are either noise peaks or R-peaks. If a detected peak meets the criteria, that is, its amplitude is greater than the noise and signal threshold, the peak is at least 200ms apart from the last detected peak, it is

not a T wave, only then it will be classified as a R peak. the noise thresholds and signal thresholds will continually be updated depending on the amplitude of the detected peaks according to Pan & Thompkins [18].
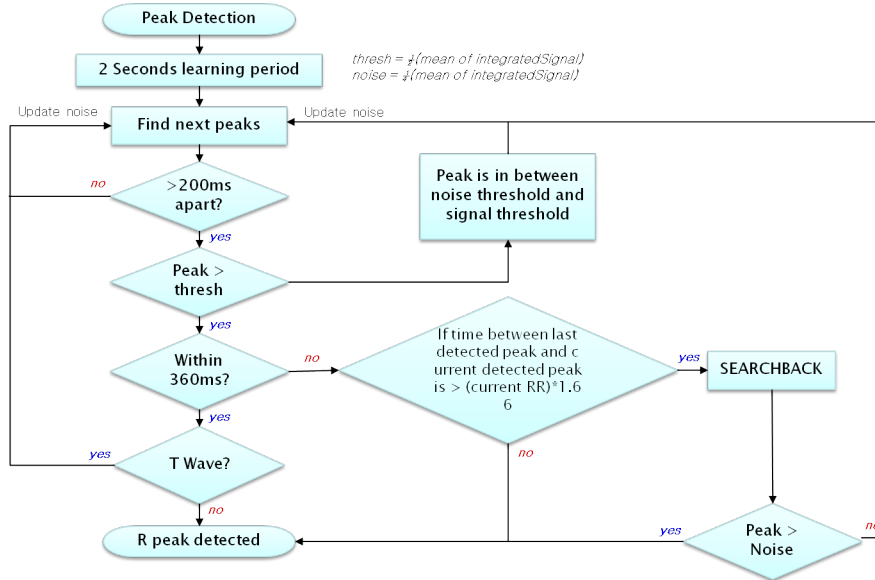
Figure 3.3: Peak sorting algorithm

3.4 Respiration Signals

3.4.1 Nasal Sensor

A simple respiration sensor was developed with the intention of comparing the EDR signals. A digital thermistor,DS18B20 by Maxim Integrated, attached to a pair of glasses, was held close to the nostrils. The sensor was comfortable and the user could wear it for long periods of time . The data from the sensor was acquired using an Arduino UNO, Figure 3.4. Figure 3.5 shows an example of how someone would wear the sensor. A compromise was reached between accuracy and speed with this particular sensor. At the end a resolution of 11 bits was chosen which allowed temperature changes of $0.065°$ and a sampling rate adequate for measuring respiration.

The result of using a peak detection based on the Pan & Thompkins al-
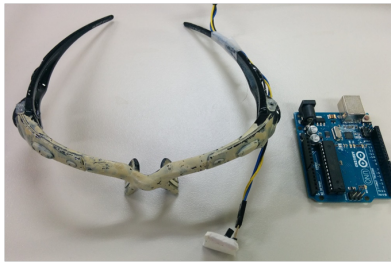
Figure 3.4: Nasal thermistor and arduino

Figure 3.5: User of nasal thermistor

gorithm is shown in Figure 3.6. The small circles which emcompass the first plot are the locations of where the R-peak were detected and hence where the MEA was calculated. Furthermore, to join the points that give a smooth signal, a cubic spine interpolator was utilised. The middle figure is the MEA derived using the wavelet transforms to detect the R-peaks, here too a cubic spline interpolation was employed to produce the smooth signal as shown. In comparison with the Pan & Thompkins method which found the area QRS complex area from the Q to S points, the latter algorithm calculates the QRS complex area by centering a 60ms window on the R-peak, the reason for this is that the Q and S peaks were not found using the wavelet transform algorithm. Lastly the third plot corresponds to that taken from the nasal thermistor. To conclude this chapter both method produced satisfactory results and show the general motion of respiration
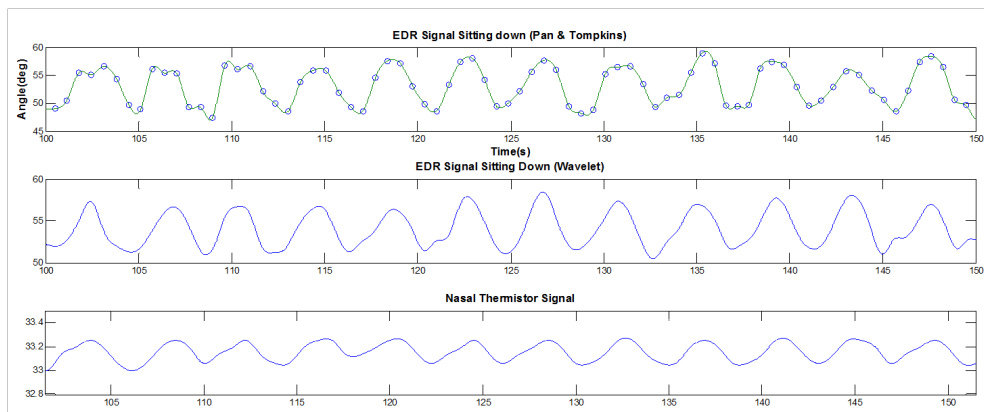
Figure 3.6: Top EDR signal, bottom, Respiration Signal

Chapter 4

Heart Rate Variability

As an appropriate transition from the covered topics about the electrocardiogram, this next section deals with Heart Rate Variability (HRV). I will briefly review the nervous system interaction in the cardio respiratory system and the modulation of the heart rate via the respiration during Respiration Sinus Arrhythmia (RSA). Also to be discussed are numerical techniques which will be used to quantify HRV, both in time and frequency domain. Indices of HRV are used as indices of cardiac autonomic regulation in both health and disease.

4.1   Autonomic Nervous System

The nervous system can be divided into the somatic and Autonomic Nervous System (ANS). Each of these systems consists of components from both the central and peripheral nervous system. The ANS is further divided into two branches, the Sympathetic Nervous System (SNS) and the Parasympathetic Nervous System (PNS) nervous system that non-voluntarily control all the organs and systems of the body. To survive, animals and humans alike must have a "fight or flight" response, this is mainly regulated by the SNS, which promotes arousal, defence and escape, whereas the PNS promotes eating and procreations. As you can see the two branches have opposite roles and work against each other in their effect on target organs, but in actuality during

everyday life the different divisions of the ANS are tightly integrated. The SNS and PNS systems are often partners in the regulation of end organs. In most cases, ranging from the simplest reflexes to more complex behaviours.

In our case, the study of the branches of the autonomic nervous system is relevant for a number of reasons. The modulation of the heart by the ANS is twofold. Sympathetic stimulation will increase heart, stroke volume, systemic vasoconstriction etc. On the other hand the PNS causes the complete opposite on reaction on the heart. The response time of the autonomic divisions greatly varies.

4.1.1 Heart Rate variability HRV

HRV describes the variations between consecutive heart beats; variations in either heart rate or the RR interval duration. The RR interval is measured between the detected R-peaks of the ECG. Clinically HRV is used as a measure of the level of health status, for instance, low HRV is associated with poorer prognosis for a wide range of clinical conditions, while on the other hand high changes in R-R interval are often associated with good health [5].

4.1.2 Respiration Sinus arrhythmia

Figure 4.1: Respiratory Sinus arrhythmia
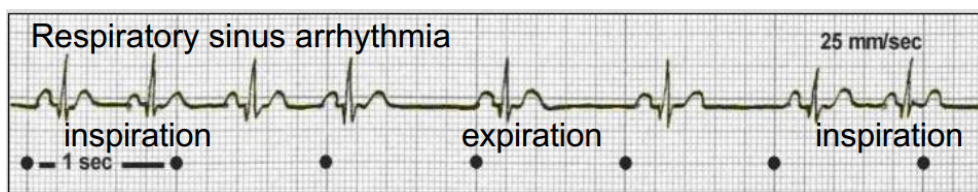
At rest, heart rate increases on inspiration and decreases on expiration. This variation of beat to beat interval which occurs during the respiratory cycle is referred to as respiratory sinus arrhythmia or RSA. RSA is measured as the difference between the shortest RR interval, RRI, during inspiration and the longest RRI during expiration in milliseconds. As we will see in the

next section changes in RSA amplitude are interpreted as changes in cardiac vagal tone.

4.1.3 Physiological origins of heart rate variability

Parasympathetic influence on heart rate is mediated via release of acetylcholine, which is released by postganglionic parasympathetic terminals at the SA node. This results in the reduction of heart rate by the binding of Acetylcholine at the muscarinic cholinergic receptors and activating a transmembrane potassium channel. The sympathetic influence is mediated by the release of epiephrineand norepinephrine, which results in an acceleration and the slow diastolic depolarization [3]. Sympathovagal activity, indicates the activity of both branches of the autonomic nervous system, ANS. Vagal tone is synonymous with the level of activity of the parasympathetic nervous system, associated with the vagus nerve or the tenth cranial nerve. The cardiac sinoatrial node, which sets the rhythm of the heart, is directly innervated by both sympathetic and vagal efferents, which exert opposing effects on the chronotropic state of the heart. The frequency response of both branches of the ANS is that of a low pass filter; the cut off frequency of the parasympathetic being 0.15Hz without delay and the sympathetic 0.015Hz with a slight 1-2 second response delay, moreover the divisions of the ANS are tightly integrated, that is, they may co-vary reciprocally, independently, or non-reciprocally [3]. Neural mechanisms far overshadow non-neural determinants of RSA. Interestingly even if there is no breathing present, RSA will persist. This was shown even after pulmonary reflexes were eliminated by deafferation [3]. Studies have pointed to the central "respiratory generator" which is linked to changes in centrally driven phrenic (respiratory) nerve activity [4]. Changes in tonic vagal activity may yield corresponding changes in RSA amplitude. This relationship however, permits strong inferences from RSA to vagal tone only to the extent to which cardiac vagal tone is the sole determinant of RSA. Inhibitory mecha-

nisms, such as central inspiratory activity, stretch reflexes from lungs and thorax and the Bainbridge reflex, alongside inhibitory and excitatory activation of the parasympathetic outflow by modulation of baro-chemoreceptor activity caused by fluctuations in arterial pressure and Pco2; are contributors to RSA [9]. Autonomic outflows can be modulated via information coming from autonomic afferents, for example, to the response of baroreceptor reflexes, which operate phasically within the rapid time frame of even the highest heart rate rhythms and exert powerful inhibitory influences on sympathetic outflow and provide an important source of excitatory drive to vagal motor neurons [3]. In a baroreceptor reflex, increase in blood pressure stimulate receptors which send impulses to the nucleus solitarius, this results in decreases sympathetic activity, which in turn decreases contractility, heart rate, and vascular tone, and increase in parasympathetic activity. [22] Sympathetic and vagal nerve activities vary throughout the respiration cycle due to the influence of reflex networks of the nucleus tractus solitarius which are modulated by respiratory influences of both central and peripheral origin, therefore respiratory modulation of autonomic nerves is proportional to the basal activity of the afferent nerves which are modulated by baroreceptor activity. Respiration gates the effect of afferent inputs on muscle sympathetic and vagal motorneurons. At usual breathing frequencies, autonomic sensory inputs are more likely to influence sympathetic and vagal firing when they arrive during expiration than at inspiration. The pulses arriving to the SA Node from the autonomic innervation, thus, are influenced by these respiration modulated afferent inputs. Due to the response of the autonomic-cardiac innervation, that of a low pass filter, the resulting RSA frequency is actually different to the breathing rate. The parasympathetic influence on the SA Node has more time to achieve full effect and dissipate at lower breathing rates, that is, the majority of respiratory influenced heart rate variability is caused by changes in vagal cardiac nerve traffic. Almost complete elimination of RSA was done by induced pharmacological cholinergic blockade

(parasympathetic blockade) of functional vagotomy (eliminated all heart rate fluctuations above 0.15) but is hardly attenuated by beta adrenergic blockade. In conclusion parasympathetic activation gives rise to fluctuation of heart rate variability at frequencies higher than 0.15Hz, during inspiration the blockade of parasympathetic activity gives rise to RSA and therefore an indicator of parasympathetic activity.

4.1.4   HRV frequency bands

Power spectral analyses have been widely used to study the periodic components of HRV. Periodic fluctuations are generally divided as shown in the table below. Table 4.1's last column described generally, the autonomic division that generates such oscillations.

Frequency band	Range	Origin
High frequency (HF)	0.15-0.4Hz	Parasympathetic
Low frequency (LF)	$0.003 - 0.04$Hz	Sympathetic and parasympathetic
Very Low Frequency (VLF)	$0.003 - 0.04$Hz	Humoral factors
Ultra Low Frequency	$0 - 0.003$ Hz	Generally omitted

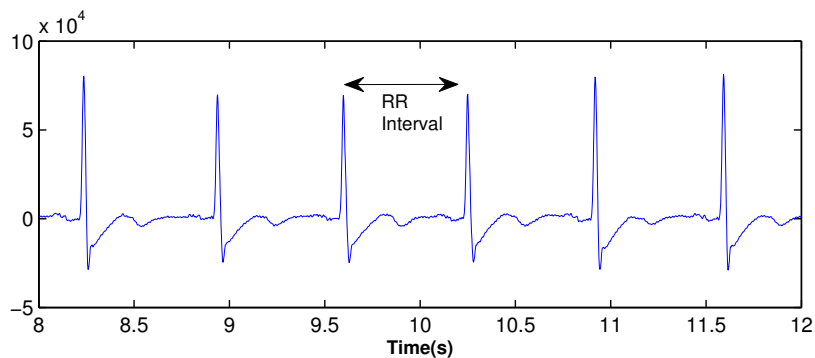Table 4.1: Frequency band designations

Figure 4.2: RR interval

Heart rate variability has been described as a marker of autonomic activity [6] Quantification and interpretation of heart rate variability depend not only
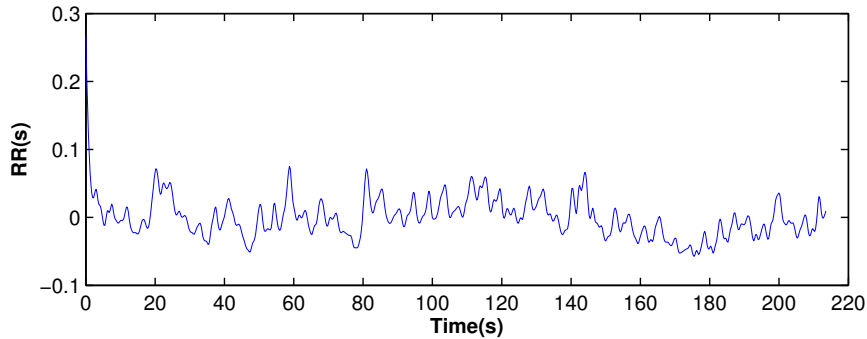
Figure 4.3: RR interval time series

on an adequate appreciation of the underlying physiological mechanisms but also on the interaction between these mechanisms and behavioral processes

4.1.5   RSA and vagal tone

Now that we have discussed the origins of RSA, this part, treats the subject of RSA as a measure of vagal sympathetic activity. Other Factors that affect cardiac vagal tone is not a constant for an individual but changes greatly as a consequence of age, posture and metabolic activity and other factors.

The study Mark Kollai was important on the findings of the relations between RSA and parasympathetic activityciteKollai1989. Parasympathetic control, measured as the change in heart rate after parasympathetic blockade, showed a proportional correlation with RSA, measured as the difference between maximum and minimum heart rate periods in a given respiratory cycle, this correlation proved to be significant but not close (r=0.61)[9]. The relationship showed that in subjects with high RSA the corresponding parasympathetic control value was also higher. The study also showed very similar results by performing the same experiment with sympathetic blockade. The authors concluded, in humans the inspiratory level of parasympathetic activity was not reduced to zero, and more importantly that parasympathetic activity levels during inspiration and expiration are altered by the respiratory pattern in co-operating human subjects; it was observed that for slower and deeper

respiration parasympathetic activity levels were higher.

4.1.6 RSA and respiration

Slower and deeper breathing rate increase the magnitude of RSA . Alterations in respiration rate and tidal volume had profound effect upon RSA magnitude that were unrelated to directly determined levels of cardiac tone. Inspiratory level of parasympathetic activity was not reduced to zero during normal quiet breathing Respiratory modulation of cardiac parasympathetic activity is different to that observed in anaesthetized dog, variation in the amplitude of respiratory sinus arrhythmia do not necessarily reflect proportional changes in parasympathetic control.

Paradoxically, as RSA increased by reduced respiration rate, in some cases, higher mean heart period, HP, was not observed as it would be believed to be so. Sometimes minimum HP's were shortnened, sometimes maximum HP's were longer or the mean HP remained unchanged.

1. Type A, whereby the mean HP shortened, due to the shortening of the minimum HPs.

2. Type Z subjects whereby the lengthening of the maximum HPs was observed and so the mean HP increased, and hence the opposite of type A.

3. In the last type, A/Z, mean HP remain unchanged.

The regression of HP on RSA for the representative RSA pattern are shown in the lower parts of Figs 1 and 2. the slope of regression ΔHP/ΔRSA ratio was negative for type A and positive for type Z and closer to zero for type A/Z. For the subjects after propanolol administration, the ratio of ΔHP/ΔRSA changed very little even after the mean HP and the magnitude of the RSA increased.

According to Kollai, during the inspiration period of subjects belonging to Type A subjects were likely to have a high parasympathetic activity, due to

the shortening of the HP during the inspiration phase where the inhibition was high. The opposite is true of type Z who probably had lower parasympathetic activity. Additionally in this study, a significant but not strong relationship was found between Parasympathetic Control (PC) and RSA. PC was measured after measuring the change in mean HP after the administration of atropine sulphate which completely blocks parasympathetic activity. Subjects belonging to the type A group showed greater PC values since patients with high PNS activity would show greater change when their PNS is disturbed. The individual responsiveness of RSA, expressed ΔHP/ΔRSA, during slow breathing was compared against the PC value for each subject. The relationship is of inverse proportionality indicating that type A subjects (high PC) have high resting (slow breathing) vagal tone and type Z subjects have low resting vagal tone.

In contrast to the modulation of cardiac parasympathetic activity in the dog, in humans, inspiratory level of parasympathetic activity is not reduced to zero. Since min HP attained during inspiration was further reduces by further interventions (handgrip, deep breathing). In addition Kollai arrived at the conclucion with his data that expiatory and inspiratory levels of parasympathetic activity are influenced by the respiration pattern in cooperating humans subjects: slower and deeper respiration was associated with higher levels of parasympathetic activity during the expiatory phase and with more effective inhibition during the inspiratory phase. This is a well known fact.

4.2   Heart rate variability measurements

Time domain measures, which are easy to calculate but don't provide as much information as frequency domain measures.

Only normal consecutively detected QRS complex, NN intervals, should be used when calculating any of these measures. Any abnormal beats should

Variable	Units	Definition
TIME DOMAIN MEASURES		
a. Statistical		
SDNN	ms	SD of all normal R–R intervals
SDANN	ms	SD of the average normal R-R intervals calculated over short time periods (usually 5 min) for the entire recording period (usually 24 h)
RMSSD	ms	The square root of the mean squared differences between adjacent normal R-R intervals
SDNN index	ms	Mean of the SD of the normal R-R intervals calculated over short periods of time (usually 5min) for the entire recording period (usually 24 h)
NN50		The number of adjacent normal R-R interval that differ by more than 50ms
pNN50		NN50 divided by the total number of normal R-R intervals x 100
b. geometrical		
HRV triangular index		Number of normal R-R intervals divided by the height of the histogram of all the normal R-R intervals measured on discrete scale with bins of 1.128s
TINN	ms	Baseline width of the minimum square difference of triangular interpolation of the highest peak of the histogram of all normal R-R intervals
FREQUENCY DOMAIN MEASURES		
Total	ms^2	Area under the entire power spectral curve(usually $\leq$0.40), variance of all normal R-R intervals
ULF	ms^2	Ultra low frequency power ($\leq$0.003Hz)
VLF	ms^2	Very low frequency power (0.003-0.04)
LF	ms^2	Low frequency power(0.04-0.15Hz)
HF	ms^2	High frequency power (usually 0.15-0.40Hz)
LFnu	nu	Normalized low frequency power (LF/LF + HF)
HFnu	nu	Normalized high frequency power (LF/LF + HF)

Table 4.2: HRV time domain and frequency domain measures

be excluded. Due to the ease of calculation, standard deviation of the NN intervals, is widely

Investigators also started relying more on measures to derive the spectral power for a given frequency band. Common spectral analysis approaches are fast Fourier transform analysis and autoregressive (AR) modelling. The frequency domain measures are used below and the last one is used as an index of autonomic nervous system balance.

4.3 HRV signal derivation

Once the ECG signal was acquired and processed and the QRS complex detected, the sequence of RR intervals as a function of R_i can be calculated the following way: R_i - R_{i-1}, this is referred to as the discrete event series (DES). Since this signal is not sampled at regular intervals a cubic spine interpolation was used to get the signal, which is necessary to calculate the spectrum of the HRV signal. Frequency of the interpolated signal was 4Hz as the Nyquist frequency at this rate is high enough for the frequencies of interest, chiefly the

LF and HF band.

Detrending

Slow trends that permeate the series can be detrimental to spectral analysis and lead to misinterpretations. For accurate spectral analysis, therefore, the signal should be as stationary as possible. Non stationaries can be reduced by keeping the subjects and conditions as stable they could be [3]; permeating slow trends can introduce the error in the HF and LF bands and result in wrong values of sympathovagal balance, ratio of LF and HF. Typically the LF band is more easily influenced than the HF band [10]. In this study it was found that the mean and SD of the LF and HF bands decreased after detrending, specially LF which changes as much as 20%. It makes sense to choose a cut of frequency that does not affect the bands of interest, Li *etal.* [10], kept the cut of at f<0.04.

Prevalent slow nonstationarities can be reduced by applying carefully constructed bandpass filters in the frequencies of interest. For this work, a detrending algorithm based on the work by Tarvainen *el al.* [13], was employed. The algorithm is based on the smoothness priors approach which, primarily is a normal distribution theory linear model;stochastic regression treatment of stationary and nonstationary time series [8]. The result is a time varying FIR filter which can have its cut off frequency modified by a single parameter λ, higher values of λ correspond to lower cut-off frequencies.

Power Spectral Density Calculation

HRV literature present two different types of methods for calculating the power spectrum density, PSD, of the HRV signal. The first type are the parametric methods, these provide smoother spectral components and easy post processing of the spectrum, however, they require a suitable model and complexity. On the other hand non-parametric methods are based on FFT algorithms which

make them very fast and simple. The following power spectral and the rest of the HRV PSD calculations plots will be based on the latter type. The non-parametric method based on the Welch power spectral density estimate was used for calculating the PSD. The key idea behind the Welch periodogram method is to divide the signal into a series of windows or segments, these segments can be overlapped and the average of the PSD of the overlapped segments calculated. More averaging reduces the error variance and provides smoother PSD curves than a simple FFT. Excess overlapping, above 75% of the segment size, would increase the number of averaging segment but this would have no added benefit since greatly overlapped segments are essentially the same and averaging them no longer effectively reduces the error variance.

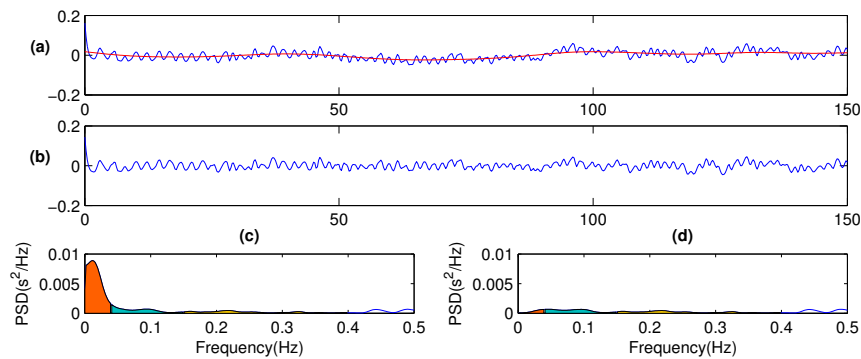Figure 4.4: Detrending the HRV time series signal and performing spectral analysis. a) HRV time series with slow trend shown in red, the trend was obtained using the Smooth priors method and in b)this signal is removed. c) and d) are the power spectrqal density plots of the raw HRV signal and the detrended singnal respectively.

In Figure 4.4

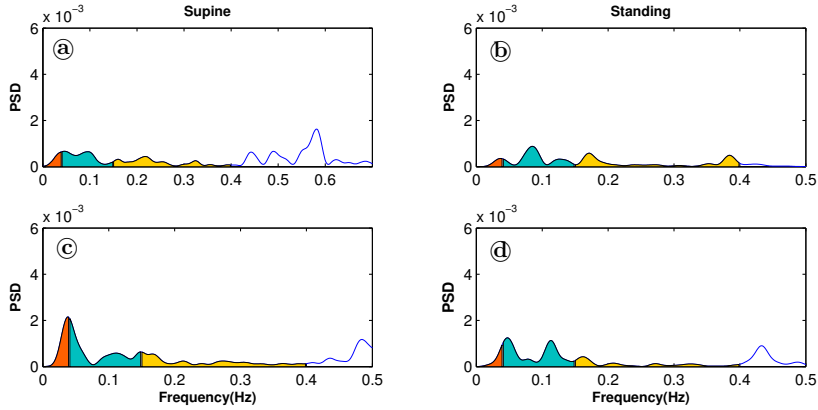## 4.3.1 Autonomic nervous system changes during supine and standing positions

Figure 4.5: Orthostatics Result, plots **a**, **c** correspond to the supine results for each subect respectively. Plots **b** and **d** coincide with the standing power spectral results. All the HRV signals that were used to derive these PSDs had the low trend removed.

	Spine	Standing
LF	40.58	30.41
HF	37.46	30.74
LF/HF	1.08	0.98

Table 4.3: Subject 1 results

	Spine	Standing
LF	54.06	52.34
HF	40.62	20.27
LF/HF	1.33	2.58

Table 4.4: Subject 2 results

Changing posture can generate more sympathetic activity, more specially during change from supine to standing. Therefore this change in posture will result in higher contribution in the LF part of the spectrum A change in $90°$ from supine to standing during a orthostatatics test, will generally show as an increase in the LF and a decrease in the HF component of the HRV part of the spectrum [14]. Increase sympathetic activity results in heart rate accelaration in the upright position and vagal withdrawal in the neural moduilation of sinus node pacemaker activity [19]. During graded orthostatic test, in which the tilt angle was $15°$, $30°$, $45°$, $60°$ and $90°$, this author found a strog correlation between the angle and the power HF and LF bands.

An orthostatic test was performed in two subejcts; the experiment consisted in a short 5 minute ECG recording with the subjects laying down, after which another 5 minutes of standing position recordings where taken. The aim was to see how the frequency bands of the HRV signals changes with

changing position. Figure 4.5 shows two plots for each subject, one for supine and the other for standing measuremnts. In general for both subjects the HF decreases, which is what we expected. As well as an apparent change in sympathetic activity showed great changes between positions; there is as much as 25% decrease in the LF band for the fist subject which paradoxically indicated that both parasympathetic and sympathetic activity decrease. In fact both bands appear to decrease when the subjects change postion. The ratio of LF/HF which indicated sympathovagal balance, differs in both subjects. In the first subject the results dont' seem to agree with the theory and show that there is more sympathetic activity than parasympathetic activity during standing. For the second subject the ratio increases during the standing measurement, which is in accordance with the theory, in this case, it must be noted the LF/HF ratio changes quite drastically between positions. This might suggest that on the second subject the heart rate increases more when changing positions as opposed to the first subject, which seems to have a more desirable sympathovagal balance of between the ANS and PNS as the ratio stays almost the same throught the experiment.

Chapter 5

Analysis and Discussion

The project dealt chiefly with topics about heart signal processing. The report starts with a few fundamental topics about the heart and the hardware required to get a good ECG. The robust ECG signal acquisition hardware which was developed could easily be adapted for electroencephalography or electrooculography measurements. The second part covering wavelet transforms theory highlights its usefulness in bio-signal processing. Raw ECG signals were denoised using wavelet transform multi resolution analysis and furthermore the QRS detector using the DWT subband coding algorithm performed satisfactorily in stored ECG data. EDR or ECG derived respiration signal was demonstrated in real-time by employing the QRS detector based on the Pan and Tompkins algorithm, although the algorithm has the advantage of detecting the Q and S points, and hence making the QRS area calculation more straightforward; the obtained EDR signal was comparable to the one derived using the wavelet transform algorithm. Future work, could involve the developing of a real-time wavalet algorithm that not only detects the R-peak but also the Q and S points before calculating the EDR signal. An ECG system that measures the respiration signal in a real time manner could be employed in a vital signs monitoring system, or in a sleep monitoring setting when taking polysomnographic measurements. Information for the evaluation of the state

of the autonomous nervous system can easily be extracted with the heart rate information, with the locations of the R-peaks; the ratio of the low frequency to high frequency power spectra, representing a measure of autonomic balance was evaluated for two subjects during an orthostatic test. Although a complete system of HRV signal derivation, de-trending and spectral analysis was developed, tests on more than two subjects, and additional data comparison with more established methods would be required to improve the quality of the results.

Bibliography

[1] Electrocardiography devices.

[2] Paul S Addison. Wavelet transforms and the ecg: a review. *Physiological measurement*, 26(5):R155, 2005.

[3] G G Berntson, J T Bigger, D L Eckberg, P Grossman, P G Kaufmann, M Malik, H N Nagaraja, S W Porges, J P Saul, P H Stone, and M W van der Molen. Heart rate variability: origins, methods, and interpretive caveats., November 1997.

[4] G G Berntson, J T Cacioppo, and K S Quigley. Respiratory sinus arrhythmia: autonomic origins, physiological mechanisms, and psychophysiological implications., March 1993.

[5] George E Billman. Heart rate variability - a historical perspective. *Frontiers in physiology*, 2(November):86, January 2011.

[6] Task force of the European society of cardiology, the North American society of Pacing, and electrophysiology. Heart rate variability - standards of measurments, physiological interpretation, and clinical use. *European Heart Journal*, 17:354–381, 1996.

[7] C Gamo, P Gaydecki, A Zaidi, and A Fitzpatrick. An implementation of the wavelet transform for ecg analysis. In *Advances in Medical Signal and Information Processing, 2000. First International Conference on (IEE Conf. Publ. No. 476)*, pages 32–40. IET, 2000.

[8] W. Gersh. *New Directions in Time Series Analysis. Part II*, chapter Smoothness Priors, pages 113–146. Springer-Verlag, 1991.

[9] Mark Kollai and Gabor Mizsei. Respiration Sinus Arrhythmia is a limited measure of cardiac parasympathetic control in man. *Journal of Physiology*, pages 329–342, 1989.

[10] Changchun Liu Liping Li, Ke Li and Chengyu Liu. Comparison of detrending methods in spectral analysis of heart rate variability. *Research Journal of Applied Sciences, Engineering and Technology*, 3(9):1014–1021, 2011.

[11] Jaakko Malmivuo and Robert Plonsey. *Bioelectromagnetism: principles and applications of bioelectric and biomagnetic fields.* Oxford University Press, 1995.

[12] RJE Merry and M Steinbuch. Wavelet theory and applications. *A literature study, Eindhoven University of Technology*, 2005.

[13] Perttu O. Ranta-aho Mika P. Tarvainen and Pasi A. Karjalainen. An advanced detrending method with application to hrv analysis. *IEEE Transactions on Biomedical Engineering*, 49:172 – 175, 2002.

[14] N. Montano, T. G. Ruscone, a. Porta, F. Lombardi, M. Pagani, and a. Malliani. Power spectrum analysis of heart rate variability to assess the changes in sympathovagal balance during graded orthostatic tilt. *Circulation*, 90(4):1826–1831, October 1994.

[15] George B Moody, Roger G Mark, Andrea Zoccola, and Sara Mantero. Derivation of respiratory signals from multi-lead ecgs. *Computers in cardiology*, 12:113–116, 1985.

[16] Lorraine T. Nott. "the cardiac cycle and the conduction system".

[17] Hannu Olkkonen. *Discrete Wavelet Transforms-Biomedical applications.* Intech, 2011.

[18] J Pan and W J Tompkins. A real-time QRS detection algorithm. *IEEE transactions on bio-medical engineering*, 32(3):230–6, March 1985.

[19] Rushmer RF. *Cardiovascular Dynamics.* WB Saunders Co, 1976.

[20] Jasjit Suri, Jos AE Spaan, Shankar M Krishnan, et al. *Advances in cardiac signal processing.* Springer, 2007.

[21] Nitish V Thakor, John G Webster, and Willis J Tompkins. Estimation of qrs complex power spectra for design of a qrs filter. *Biomedical Engineering, IEEE Transactions on*, (11):702–706, 1984.

[22] Thomas. Cardiac Physiology.

[23] John Webster. *Medical instrumentation: application and design.* John Wiley & Sons, 2009.

[24] Huabin Zheng and Jiankang Wu. A real-time qrs detector based on discrete wavelet transform and cubic spline interpolation. *TELEMEDICINE and e-HEALTH*, 14(8):809–815, 2008.

초록

호흡수 측정과 심박변이 분석을 위한 심전도 신호 처리

성 명 Joaquin Sanchez Duarte

학과 및 전공 전기컴퓨터 공학부

서울대학교 대학원

이 논문에서는 먼저 전반적인 ECG 신호 처리 방법에 대해 조사하였 으며, 개발한 실시간 ECG 신호 처리 장치를 이용한 신호 처리 방식과 기존의 방식과의 노이즈 감쇄, 베이스 라인 제거 성능을 비교하였다. QRS 검출을 위해서는 비 실시간으로 웨이블릿 트랜스폼 방식을 사용하였으며, 실시간 상에서는 Pan과 Tompkins에 의해 개발된 모듈 감지 방식을 사용하였다. R 피크 검출 알고리즘과 갈비뼈 부분의 비침습적으로 부착된 추가적인 전극을 이용하여 심장의 혈류량을 측정함으로써 호흡 신호를 유추할 수 있었다. 마지막으로, R 피크 검출 알고리즘을 통해 R 피크 간의 간격인 심장 박동률을 검출하였다. 심장 박동률의 통계적인 분석과 스펙트럼 분석으로 생리, 심리적 연구에 유용한 자율신경계에서 심장 박동 조절에 관한 틀을 만들 수 있었다.

주요어 : ECG, 웨이블릿 트랜스폼, Pan & Tompkins, 호흡신호, 실시간

학번: 2012-23961